International Journal of Mass Spectrometry 457 (2020) 116426

Contents lists available at ScienceDirect

International Journal of Mass Spectrometry

journal homepage: www.elsevier.com/locate/ijms

Feature article

Thermalisation of C_2^- with noble gases in cold ion traps

Barry P. Mant [a], Franco A. Gianturco [a, *], Roland Wester [a], Lola González-Sánchez [b], Ersin Yurtsever [c]

[a] Institut für Ionenphysik und Angewandte Physik, Universität Innsbruck, Technikerstr. 25, 6020, Innsbruck, Austria
[b] Departamento de Química Física, University of Salamanca, Plaza de Los Caídos Sn, 37008, Salamanca, Spain
[c] Department of Chemistry, Koç University, Rumelifeneri Yolu, Sariyer, TR-34450, Istanbul, Turkey

ARTICLE INFO

Article history:
Received 29 July 2020
Received in revised form
21 August 2020
Accepted 21 August 2020
Available online 6 September 2020

Keywords:
Ion traps
Inelastic scattering
Potential energy surfaces
Quantum dynamics

ABSTRACT

The potential energy surfaces for C_2^- ($^2\Sigma_g^+$) interacting with He, Ne and Ar are calculated using *ab initio* quantum chemistry methods. The PES are used to carry out coupled-channel quantum scattering calculations for the three systems to obtain the rotationally inelastic scattering cross sections from which the rotationally inelastic state-changing rate coefficients are computed. These rate coefficients are then used to compute thermalisation times of C_2^- in an ion trap employing He, Ne or Ar as different, and possible, buffer gases. A detailed analysis of their comparative collisional efficiencies is presented for guidance in trap modeling studies.

1. Introduction

Arguably the most studied molecular anion is C_2^- [1–24] but despite decades of research, it is still of interest as a potential candidate for laser cooling [25–28] which has so far not been achieved for a charged molecule. The low lying excited electronic states $A^2\Pi_u$ and $B^2\Sigma_u^+$ of C_2^- have favourable branching ratios with the ground $X^2\Sigma_g^+$ state with Franck-Condon factors for both excited states' $v' = 0 \rightarrow v'' = 0$ transition calculated to be at least 70% [22,29]. Simulations have shown that laser cooling of C_2^- can in principle reach milikelvin temperatures using Doppler or Sisyphus cooling in Paul or Penning traps [25,26] and photodetachment cooling could allow even lower temperatures to be accessed [27]. Laser cooling of C_2^- anions could allow sympathetically cooling other anions [26] or even antiprotons [27] which could then permit the efficient production of antihydrogen atoms, the latter species currently being investigated to test fundamental principles of physics [30,31].

In a previous work we have calculated the cross sections and rate coefficients for rotationally inelastic collisions of C_2^- with helium, a partner often employed as a buffer gas in ion traps. The rates for rotational excitation and quenching were similar to those for other ionic molecules interacting with helium [32]. Helium has also been suggested as a buffer gas for initially cooling the vibrational motion of C_2^- before laser cooling [25]. As C_2^- has no oscillating dipole, the vibrational levels are long lived with the ground electronic state's $v = 2$ levels persisting for over 5 s [11]. Collisions are thus the only viable means of quenching these states efficiently. Very recently, we have carried out additional calculations for the cross sections and the rate coefficients describing the vibrational quenching of C_2^- in collisions with He. Those calculations showed that such rate constants are very small, orders of magnitudes lower than those for rotations and of the same order of magnitude as those for neutral systems. These results are currently being extended to other possible noble gases as potential buffer gas choices in a trap and will be presented elsewhere [33], to investigate other options which could be more efficient at quenching the internal motion of the C_2^- anion.

In this work we shall focus instead on the interaction of C_2^- with the noble gases helium, neon and argon, employing *ab initio* quantum chemistry methods, but when the anion's bond length is kept fixed at its equilibrium value and treated as a rigid rotor during quantum scattering calculations.

Comparing the rotational excitation and de-excitation cross sections and rate constants for He, Ne and Ar is an important step for then additionally considering vibrational quenching as in the

* Corresponding author.
E-mail address: francesco.gianturco@uibk.ac.at (F.A. Gianturco).

https://doi.org/10.1016/j.ijms.2020.116426

work currently in preparation that will be presented elsewhere [33]. The computed rotational thermalisation time which we shall discuss below will then be used to assess the efficiency of each gas to cool the internal rotational motion of the anion once taken to be already in its ground vibrational state.

The paper is organised as follows. Section 2 gives details of the *ab initio* quantum chemistry calculations used to construct analytical potential energy surfaces (PES) for each system. The PES of C_2^- interacting with He, Ne and Ar are compared with their similarities and differences discussed. Section 3 presents details of the coupled channel quantum scattering calculations for collisions of C_2^- with each of the noble gases considered. The inelastic cross sections and corresponding rate constants for rotational transitions are compared for each system. In Section 4 we model the thermalisation of C_2^- in ion traps at different cryogenic temperatures using He, Ne or Ar as a buffer gas and assess how quickly the anions rotational populations approach the Boltzmann distributions. Finally, our conclusions are given in Section 5.

2. *Ab initio* calculations and potential energy surfaces

The interaction energy between C_2^- ($^2\Sigma_g^+$) and Ne and Ar respectively, was calculated *ab initio* on a Jacobi grid with 41 radial (the distance from the centre of mass of C_2^- to the atom location) R points ranging from 2.6 to 25.0 Å and θ (the angle between R and the C_2^- internuclear axis) from 0 to 90° in 10° intervals. The radial grid included a higher density of points around the minima regions at each selected angle. The C_2^- bond length was frozen at its equilibrium value of 1.269 Å [22]. Energies were calculated using the CCSD-T method for open shell systems as implemented in MOLRPO [34,35] with complete basis set (CBS) extrapolation using the aug-cc-pVTZ, aug-cc-pVQZ and aug-cc-pV5Z basis sets [36,37]. The basis-set-superposition-error (BSSE) was also accounted for at all calculated points using the counterpoise procedure [38]. For some small values of R at small angles θ, where the potential is repulsive, some calculations did not converge. Energies for these geometries were obtained by fitting a Morse type function to the energies for each angular cut and extrapolating to small R. Details of the C_2^-–He *ab initio* PES are provided in a recent publication from our group [39].

An overview of the PES of each system is given using contour plots in Fig. 1 which also shows the potential energy V for each system at linear and perpendicular geometries. The minimum energy for each system occurs for perpendicular geometries and is: − 27 cm^{-1} at 4.5 Å for He, − 114 cm^{-1} at 3.7 Å for Ne and − 488 cm^{-1} at 3.7 Å for Ar. From Fig. 1 it can be seen that each system's PES has a fairly similar appearance with the well depth being the main difference which increases as expected from He to Ne to Ar. This is obviously due to the increasing number of electrons on the atoms and on the much larger dipole polarizability that dominates the long-range attractive terms with a value of 1.383 a_0^3 for He, 2.660 a_0^3 for Ne, and 11.070 a_0^3 for Ar [40]. It can also be seen from the contour plots of Fig. 1 that the PES for each system are fairly isotropic, particularly for C_2^--He.

The PES for each system was analytically represented by expanding it using a Legendre polynomial series as

$$V(r_{eq} \mid R, \theta) = \sum_{\lambda}^{\lambda_{max}} V_\lambda(r_{eq}|R) P_\lambda(\cos\theta) \quad (1)$$

where, because C_2^- is a homonuclear target and thus symmetric around $\theta = 90°$, only even terms of the Legendre series are required with integer label λ. Using a nine term expansion, i.e. with $\lambda_{max} =$ 16, gave a root-mean-square error to the *ab initio* data of 0.64 cm^{-1} for the C_2^-–Ne system and 1.4 cm^{-1} for the C_2^-–Ar system for geometries with potential energies below 1000 cm^{-1}.

The radial coefficients $V_\lambda(r_{eq}|R)$ for the most important terms in the expansion, $\lambda = 0, 2$ and 4, are plotted in Fig. 2. As expected the spherical V_0 term changes the most between the systems decreasing its minimum value from − 25 cm^{-1} for He, to − 100 cm^{-1} for Ne and − 422 cm^{-1} for Ar. This term mostly accounts for the greatest well depth for each system in the series. The V_2 term is also seen for each system to have a smaller minimum before increasing in value, with the depth of the minimum increasing from He to Ne to Ar. This will cause the most important $\Delta j = 2$ transition cross sections and rates to increase in the series as will be discussed below. The V_4 term is quite similar for each system and is repulsive.

The increase in well depth and corresponding decrease in value of the V_0 expansion term is similar to what is calculated for the CN^-/He and CN-/Ar systems which we have recently investigated [41]. These somewhat similar systems will be used as comparisons when discussing the thermalisation times below.

The PES and Legendre expansion coefficients for the C_2^- system interacting with noble gas atoms can be compared to the anion's interaction with the open-shell, highly polarizable atoms Li and Rb recently studied by Kas et al. [23]. For these systems, there is a far stronger interaction with the minimum of the PES at perpendicular geometries of around −18,000 and − 10,500 cm^{-1} for Li and Rb respectively. The V_0 terms reflect this with minima of around 12,000 (1.5 eV) and 8000 cm^{-1} (1.0 eV) respectively.

The expansion parameters $V_\lambda(r_{eq}|R)$ for the C_2^--Ne and C_2^--Ar PES and are provided in the supplementary information as well as the Fortran subroutines which give potential energies as a function of Jacobi coordinates for both systems.

3. Quantum scattering calculations and inelastic rate coefficients

Quantum scattering calculations for the collision of C_2^- with Ne and Ar were carried out using our in-house quantum scattering computational code ASPIN [42] with the anion treated as a rigid rotor (RR). The ground electronic state of C_2^- is $^2\Sigma_g^+$, a doublet state. The presence of the electronic spin in a doublet state splits the usual nuclear rotational levels N of a rotating molecule into doublets so that each resultant rotational level j (other than the ground $j = 0.5$) is split into two values with $j = N \pm 0.5$. The energy of the rotational levels are given as

$$\varepsilon_{jN} = \begin{cases} BN(N+1) + \frac{1}{2}\gamma N & j = N + \frac{1}{2} \\ BN(N+1) - \frac{1}{2}\gamma(N+1) & j = N - \frac{1}{2} \end{cases} \quad (2)$$

where B is the rotational constant taken as 1.74 cm^{-1} [22] and the spin-rotation constant, γ can be taken from experiment with a value of 4.25×10^{-3} cm^{-1} [8]. Although the scattering of a structureless particle from a $^2\Sigma$ state target [43] is implemented in ASPIN, we instead treat the C_2^- anion as pseudo-singlet ($^1\Sigma$). In our recent paper on C_2^--He scattering [39] we showed that cross sections and rates constants obtained from a pseudo-singlet treatment of the anion were almost identical to those obtained by summing the relevant spin-split cross sections from an explicit doublet treatment. Since the main aim of this work is to compare thermalisation times when changing buffer gas, we have carried out scattering calculations treating the C_2^- anion as pseudo-singlet.

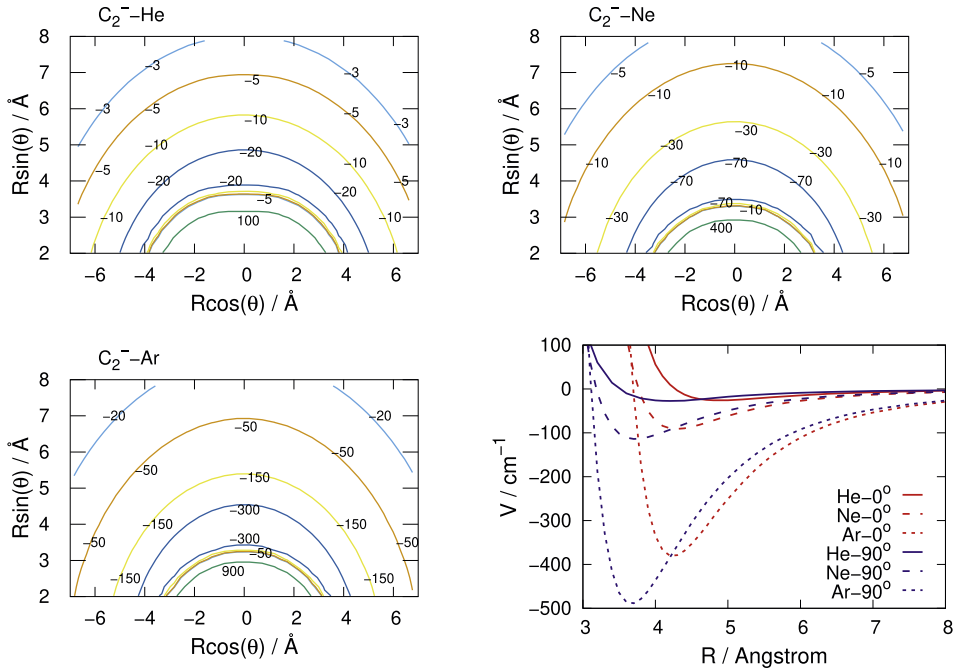

Fig. 1. Contour plots of C_2^- ($^2\Sigma_g^+$)-He/Ne/Ar PES projected onto Cartesian coordinates. Bottom right plot shows V at linear and perpendicular geometries for each system. Energies in cm^{-1}.

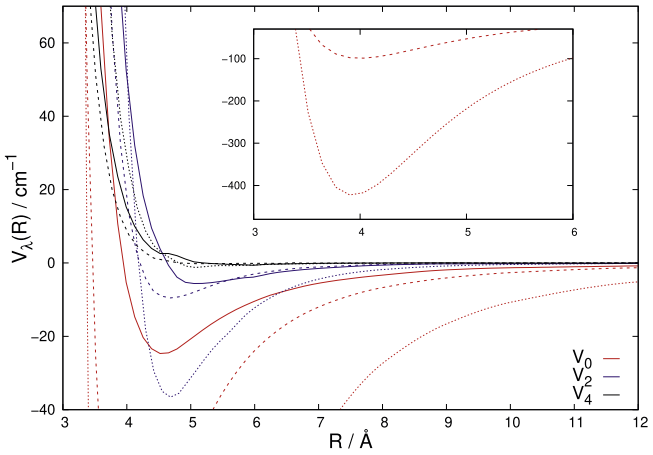

Fig. 2. Computed radial coefficients of the expansion in Eq. (1) for C_2^- interacting with He (solid lines), Ne (long-dashed lines) and Ar (short-dashed lines). Only the first three, most important radial functions are shown.

With this approximation, only even j states are required in the calculations, due to the nuclear statistics of the $^{12}C_2^-$ molecule with zero-spin nuclei.

ASPIN makes use of the Coupled-Channel (CC) method to solve the Schödinger equation for scattering of an atom with a diatomic molecule. The method has been described in detail before [42,44] and only a brief summary will be given here. For a given total angular momentum $\mathbf{J} = \mathbf{l} + \mathbf{j}$, the scattering wavefunction is expanded as

$$\Psi^{JM}(R,\Theta) = \frac{1}{R}\sum_{j,l} f_{lj}^{J}(R)\,\mathscr{Y}_{jl}^{JM}(\hat{\mathbf{R}},\hat{\mathbf{r}}) \tag{3}$$

where l and j are the orbital and rotational angular momentum respectively, $\mathscr{Y}_{jl}^{JM}(\hat{\mathbf{R}},\hat{\mathbf{r}})$ are coupled-spherical harmonics for l and j which are eigenfunctions of J. The index M indicates the projection of J onto the space-fixed axis. The values of l and j are constrained, via Clebsch-Gordan coefficients, such that their resultant summation is compatible with the total angular momentum J [42,44]. $f_{lj}^{J}(R)$ are the radial expansion functions which need to be determined. Substituting the expansion into the Schödinger equation with the Hamiltonian for atom-diatom scattering [42,44] leads to the CC equations for each J

$$\left(\frac{d^2}{dR^2} + \mathbf{K}^2 - \mathbf{V} - \frac{\mathbf{l}^2}{R^2}\right)\mathbf{f}^{J} = 0. \tag{4}$$

Here each element of $\mathbf{K} = \delta_{i,j}2\mu(E-\varepsilon_i)$ (where ε_i is the channel asymptotic energy), μ is the reduced mass of the system, $\mathbf{V} = 2\mu\mathbf{U}$ is the interaction potential matrix between channels and $\mathbf{l}^2$ is the matrix of orbital angular momentum. Scattering observables are obtained in the asymptotic region where the Log-Derivative matrix has a known form in terms of free-particle solutions and unknown mixing coefficients. Therefore, at the end of the propagation one can use the Log-Derivative matrix to obtain the K-matrix by solving the following linear system:

$$(\mathbf{N}' - \mathbf{YN}) = \mathbf{J}' - \mathbf{YJ} \tag{5}$$

where $\mathbf{J}(R)$ and $\mathbf{N}(R)$ are matrices of Riccati-Bessel and Riccati-Neumann functions [42]. From the K-matrix the S-matrix is easily obtained and from it the state-to-state cross sections. The rotational state-changing cross sections are then obtained as

$$\sigma_{j\to j'} = \frac{\pi}{(2j+1)k_j^2}\sum_{J}(2J+1)\sum_{l,l'}\left|\delta_{lj,l'j'} - S_{lj,l'j''}^{J}\right|^2. \tag{6}$$

To converge the CC equations, a rotational basis set was used which included states with up to $j = 20$ within the coupled-channel (CC) expansion. The CC equations were propagated between 1.7 and

100.0 Å in 2000 steps using the log-derivative propagator [45] up to 60 Å and the variable-phase method [46] at larger distances up to 100 Å. The convergence of the scattering calculations with respect to basis set, number of terms in PES expansion, propagation distance and number of steps was checked. The cross sections are converged to at least a few percent or better which will have a negligible effect on calculated rates. The potential energy was interpolated between calculated $V_\lambda(r_{eq}|R)$ values using a cubic spline and extrapolated below and above the *ab initio* grid using linear and polynomial functions respectively as implemented in ASPIN [42]. As our *ab initio* grid goes to 25.0 Å and the scattering energies of interest are not in the ultracold or high energy regimes, the details of the potential extrapolation have a negligible effect on the scattering cross sections. Hence, replacing the extrapolated potential from ASPIN with $V(R) = -\alpha/2R^4$ using the experimental polarizabilities given above resulted in a negligible change in scattering cross sections, even at the lowest energies considered.

Scattering calculations were carried out for the C_2^-–Ne system for collision energies between 1 and 500 cm^{-1} using steps of 0.1 cm^{-1} for energies up to 100 cm^{-1}, 0.2 cm^{-1} for 100-200 cm^{-1}, 1.0 cm^{-1} for 200-400 cm^{-1} and 2 cm^{-1} for 400-500 cm^{-1}. The C_2^--Ar cross sections have more resonance features (see below) and so the grid was slightly modified so that a spacing of 0.2 cm^{-1} for 100-300 cm^{-1} was used and 1.0 cm^{-1} for 300-400 cm^{-1}. This fine energy grid was used to ensure that important features such as resonances appearing in the cross sections were accurately accounted for and their contributions correctly included when the corresponding rates were calculated. The number of partial waves was increased with increasing energy. For the C_2^--Ne system with a reduced mass μ of 10.9068 amu, partial waves of up to $J = 124$ were used while for the heavier C_2^-–Ar system with $\mu = 14.9947$ amu, up to $J = 196$ was required at the highest collision energies considered. Inelastic cross sections were computed for all transitions between $j = 0$ to $j = 8$ which should be sufficient to model buffer gas dynamics in a cold trap up to about 100 K. Details of scattering calculations for the C_2^-–He system have been given in our previous work [39].

The rotationally inelastic excitation scattering cross sections for C_2^- colliding with He, Ne and Ar are presented in Fig. 3 for $\Delta j = 2$ and 4 transitions from the $j = 0$ and $j = 2$ rotational states. As anticipated from the discussion of the PES and Legendre expansion in Section 2, $\Delta j = 2$ transitions are by far the largest for all three systems, a reflection of the importance of the V_2 term in Eq. (1). The size of the scattering cross sections also uniformly increase on going from He to Ne to Ar as also anticipated from our discussion on the relative features of their PESs. Fig. 3 also shows how the region of scattering resonances increases in energy on going from He to Ar. This is likely due to the increasing reduced mass μ of the system resulting in the occurrence of more numerous shape-resonances in the inelastic cross sections for the heavier systems.

Rotationally inelastic de-excitation scattering cross sections are shown in Fig. 4 for various example transitions. In this case a log scale is used due to the larger range of magnitudes of the cross sections. The large de-excitation cross sections at low energies is a general feature in inelastic collisions and can be rationalised as the incoming atom having more time to interact with the molecule. As with Fig. 3, the scattering cross sections uniformly increase in magnitude on going from He to Ne to Ar due to the increasing interaction of the atoms with the anion.

The rotationally inelastic rate constants $k_{j\to j'}(T)$ can be evaluated as the convolution of the scattering cross sections over a Boltzmann distribution of the relative collision energies:

$$k_{j\to j'}(T) = \left(\frac{8}{\pi\mu k_B^3 T^3}\right)^{1/2} \int_0^\infty E\sigma_{j\to j'}(E) e^{-E/k_B T} dE. \quad (7)$$

The rate constants for the rotationally inelastic transitions corresponding to those of Fig. 3 for temperatures between 5 and 100 K are shown in Fig. 5. Following the scattering cross sections, the rate constants for $\Delta j = 2$ transitions are the largest. Unlike the cross sections however, the rate constants for He and Ne are very similar over the temperature range. This is a consequence of the reduced

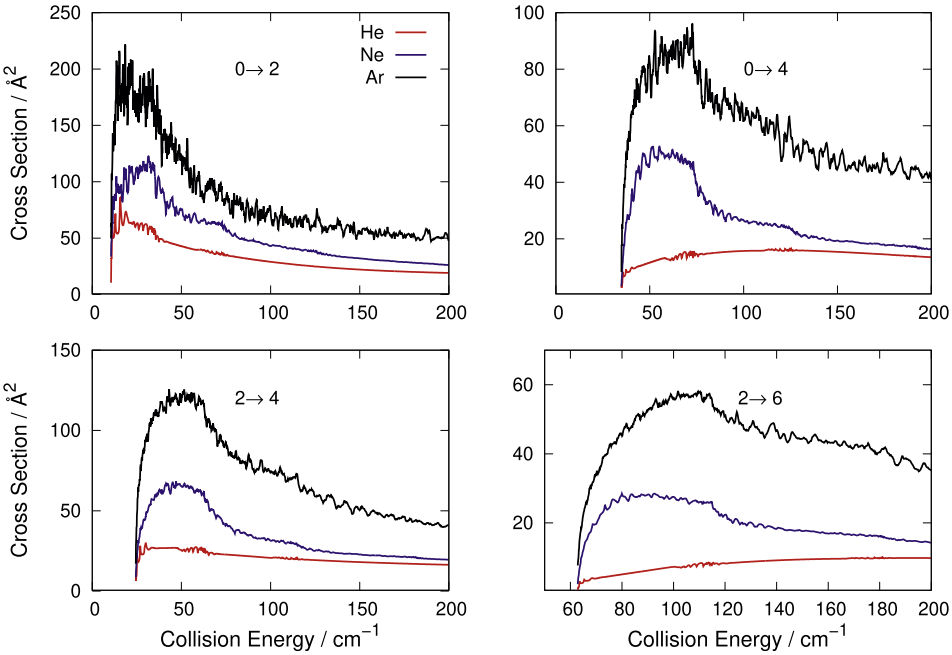

Fig. 3. Rotationally inelastic excitation scattering cross sections for C_2^- colliding with He (solid lines), Ne (long-dashed lines) and Ar (short dashed lines) for $\Delta j = 2$ (left panels) and $\Delta j = 4$ (right panels) transitions from the $j = 0$ (top panels) and $j = 2$ (bottom panels) rotational states.

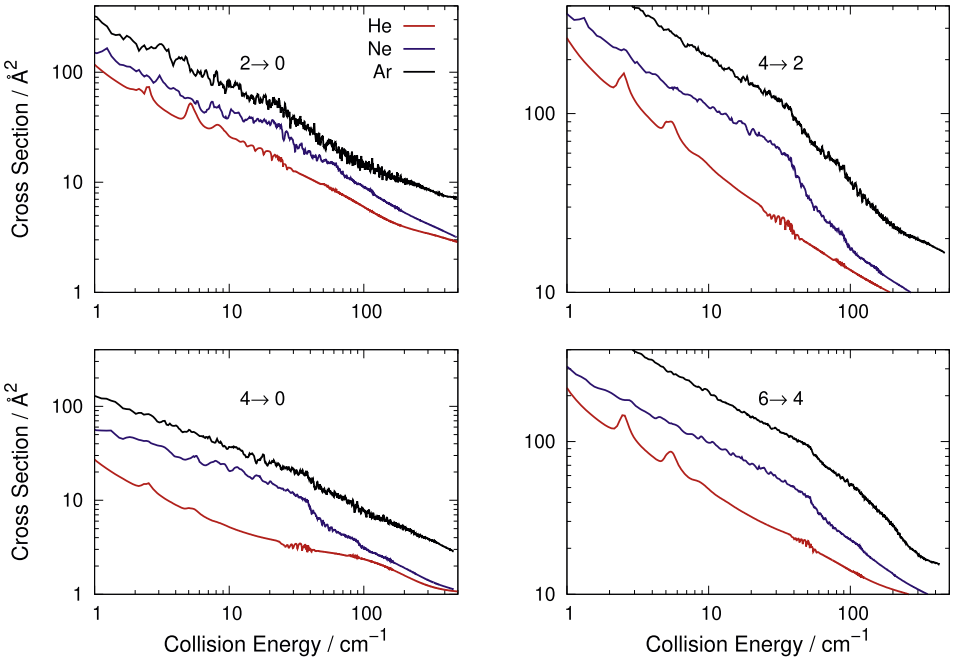

Fig. 4. Rotationally inelastic de-excitation scattering cross sections for C_2^- colliding with He (solid lines), Ne (long-dashed lines) and Ar (short dashed lines) for various transitions.

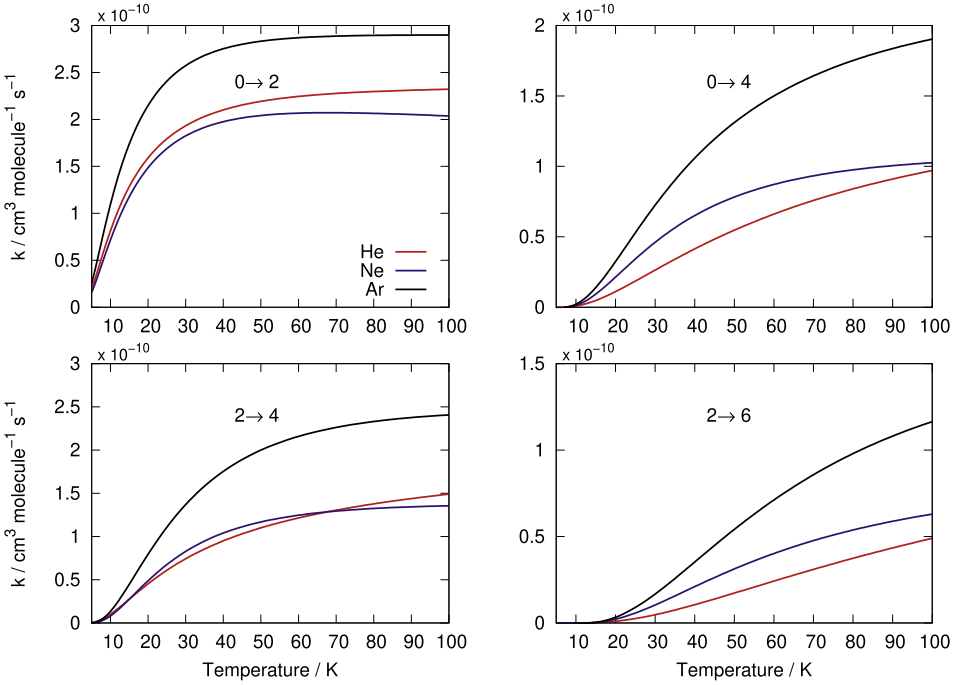

Fig. 5. Rotationally inelastic excitation rate constants $k_{j\to j'}(T)$ for corresponding transitions of Fig. 3.

mass μ which appears in the denominator of Eq. (7). Thus, although the inelastic cross sections for C_2^--Ar are large enough to ensure that the corresponding rates remain the largest despite the largest value of μ, for C_2^--Ne the larger μ is combined with only a modest increase in scattering cross sections, a feature which results in the computed rate constants being similar to those for C_2^--He. This result from our study will have implications for the thermalisation times discussed below, where the He and Ne partners of the trapped anion will be shown to give similar results under the conditions considered.

Fig. 6 shows the de-excitation rate constants corresponding to those of the transitions shown in Fig. 4. Rate constants for C_2^--Ar collisions are again the largest for all transitions. For He and Ne the situation is more complicated with the larger rate constant depending on the specific transition. For $j = 2\to0$, He has larger rate constants while for $j = 4\to0$, Ne is larger. The other panels of Fig. 6 show a temperature dependence on the He and Ne rate constants such that for both the $j = 4\to2$ and $j = 6\to4$ transitions, Ne gives the larger values at lower temperatures but then He is larger. Again, this subtle interplay of structural and dynamical

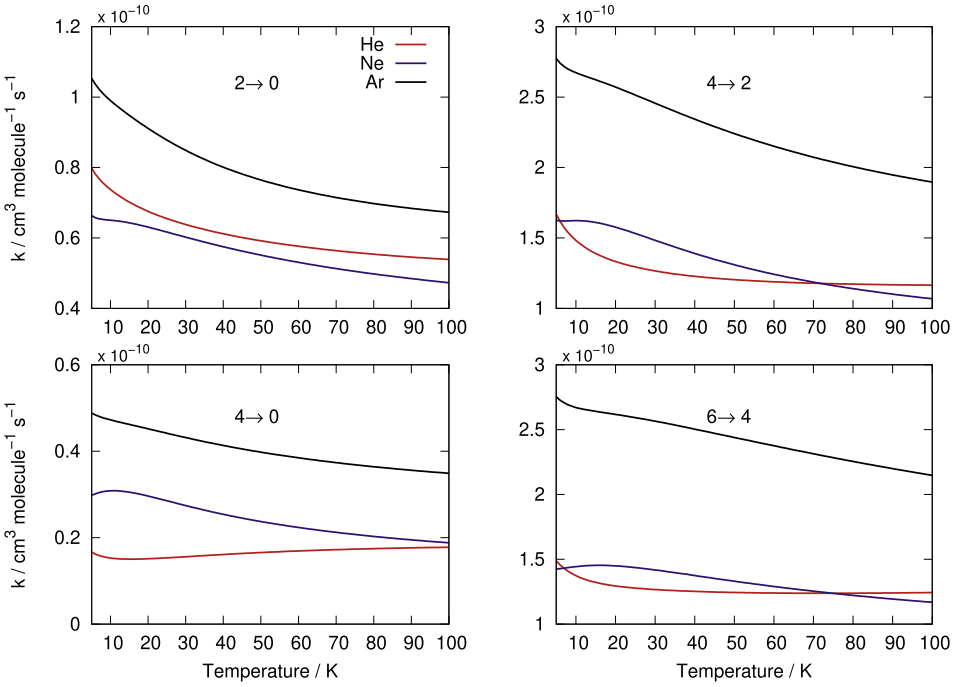

Fig. 6. Rotationally inelastic de-excitation rate constants $k_{j\to j'}(T)$ for corresponding transitions of Fig. 4.

features in driving the relative sizes of the rate constants at changing temperatures will affect the thermalisation times of C_2^- with the buffer gases, as further discussed below.

The results obtained here can be compared to similar systems. The cross sections for rotationally inelastic transitions of C_2^- colliding with Li and Rb were reported by Kas et al. [23] and were found to be quite similar to each other. The cross sections for various transitions between $j = 0$ to $j = 8$ levels varied from between 1000 and 100 Å^2. As a specific comparison, the cross sections for $j = 0$ to $j = 2$ increased rapidly near threshold (10 cm^{-1}) to around 1000 Å^2 before steadily reducing to about 80 Å^2. The above cross sections are around 4 times larger than those for the case for C_2^--Ar reported here, although they become similar in size at the higher collision energies. The corresponding rate coefficients for both Li and Rb colliding with C_2^- given in [23] vary from about 4 to 10 times larger than those reported here for the present noble gas atoms. It provides a clear example of the role played by the larger polarisabilities of the Li and Rb partners in driving the inelastic dynamics of the present anion.

The cross sections and rates can also be compared to CN^-/He and CN^-/Ar collisions which we have also recently studied [41] under similar trap conditions. The interaction potential and Legendre expansion terms for those systems are similar to those for C_2^--He and C_2^--Ar reported here but with the important distinction of being heteronuclear. A similar increase in magnitude of cross sections and rate constants was also observed for CN^- when comparing He and Ar collisions. Further comparisons with this system in relation to thermalisation times are made in the next section.

The rate constants for C_2^--Ne and C_2^--Ar for all transitions between $j = 0$ and $j = 8$ from 5 to 100 K in 1 K intervals are given in the supplementary information. Those for C_2^--He have been previously given in a separate publication [39].

4. Thermalisation times in cold ion traps

The rate constants for rotationally inelastic collisions presented in Section 3 can now be used to model the thermalisation kinetics of C_2^- molecules in an ion trap with He, Ne or Ar used as a buffer gas. To follow the evolution of the C_2^- anion's rotational state populations $n_i(t)$, the following rate equations, describing such evolution as induced by collisional energy transfer with the chosen buffer gas, are solved:

$$\frac{dn_i(t)}{dt} = \sum_{j\neq i} n_j(t) C_{ji}(T) - n_i(t) \sum_{i\neq j} P_{ij}(T). \tag{8}$$

The $P_{ij}(T)$ are the rates for the destruction of the population of level i, while its formation rates are given by the $C_{ji}(T)$ coefficients. The coefficients are given as a function of the inelastic rate coefficients and the gas density η as

$$P_{ij}(T) = \eta k_{i\to j}(T) \tag{9}$$

$$C_{ji}(T) = \eta k_{j\to i}(T). \tag{10}$$

The initial rotational populations and the collisional temperature T of the trap are parameters to be selected for each simulation's run. Eq. (8) were solved using the fourth order Runge-Kutta method. The rates due to spontaneous radiative processes are usually negligible in such simulations due to the high buffer gas pressure resulting in collisional rates being the dominant process in changing the molecule's rotational state [32]. For C_2^- this is an even better approximation since the anion has no dipole moment and thus dipole transitions are forbidden.

For ion trap experiments, often helium is employed as a buffer gas due to its low boiling point at ambient pressure of 4 K. This

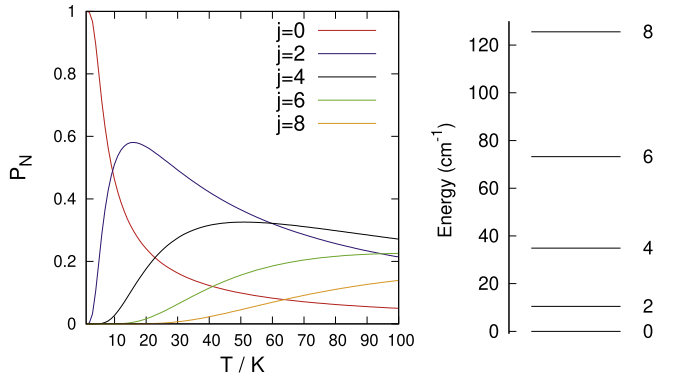

Fig. 7. Boltzmann populations of C_2^- rotational states up to 100 K (left panel) and rotational energy levels (right panel).

allows a range of trap temperatures to be chosen depending on the specific experiment [47]. Fig. 7 shows the Boltzmann distribution for the rotational states of C_2^- between 1 and 100 K and the corresponding rotational energies. For this temperature range it can be seen that rotational states between $j = 0$ to $j = 8$ are significantly populated and need to be included in the thermalisation simulations.

Fig. 8 shows the simulation of C_2^- thermalisation using He, Ne and Ar as buffer gases at 20 K. The initial rotational populations $n_i(t = 0)$ of the anion are set to those of a Boltzmann distribution at 100 K and the buffer gas density η is chosen as 10^{10} cm^{-3}, typical for ion traps [47]. The boiling points of these buffer gases are very different at ambient pressures: 4 K for He, 27 K for Ne and 87 K for Ar. The 20 K temperature for the simulation in Fig. 8 is therefore feasible for He and Ne but not Ar and the latter is included for comparison purposes. It is also of note that, under the low-pressure trap conditions the buffer gases can be employed below their boiling points without substantial losses via condensation in the trap and argon has been used as a buffer gas down to about 55 K [48].

In Fig. 8 the vertical dashed line is used to indicate the time when the rotational states reach thermal equilibrium which was defined to be when the $j = 0$ state's population n_0 remains unchanged in the fourth decimal place. This definition is the same as that chosen in our previous work on CN^-/He,Ar collisions [41] and allows comparisons to made between systems.

The populations of the rotational states for all panels in Fig. 8 approach their steady-state values shown in Fig. 7 after a time interval, a consequence of the principle of detailed balance. Thermalisation times for C_2^- with He or Ne buffer gas are similar at around 7 and 6 s respectively. This is a consequence of the similarity of the rate coefficients for rotationally inelastic transitions as discussed in Section 3. For Ar, the thermalisation time is about twice as fast at 3 s but as discussed, the use of Ar would likely not be feasible at 20 K. Nevertheless, this numerical simulation shows that the larger rate constants we had found earlier for Ar result in a correspondingly faster thermalisation dynamics.

Fig. 9 shows a similar thermalisation but for gas temperatures of 60 K, feasible for all gases. At this higher temperature, the thermalisation times are shorter as the populations are closer to their initial values at 100 K. At this temperature the thermalisation times are in order Ar < Ne < He, increasing by 2 s intervals. That Ar is the fastest is a result of the larger rotationally inelastic rate constants for all transitions. For Ne and He the difference in thermalisation times will depend on the specific temperature due to the similarity and temperature dependence of the rate constants, as discussed in Section 3.

The results presented here for C_2^- thermalisation times with He and Ar can be compared to the CN^- anion for which we have carried out similar simulations [41]. At 20 K (and for the same gas density $\eta = 10^{10}$ cm^{-3}), the thermalisation times for CN^- with He is 5 s, slightly faster than found here for C_2^-. At 60 K the thermalisation times for CN^- with He and Ar are 3 and 2 s respectively. For Ar this is the same as the thermalisation time for C_2^- but faster than for C_2^-–He at this temperature (6 s). Thus for v the same trend in thermalisation time is observed as for CN^-, namely that the larger noble gas atoms give faster times due to their stronger interaction with the anions. The specifics are different however. Probably the most important difference is that for CN^-, $\Delta j = 1$ transitions are also allowed in the collision networks and are therefore driving a different state-changing kinetics than that in the case of C_2^-.

Finally it is worth noting that for CN^- the thermalisation times for H_2 as a buffer gas were also considered and found to be even faster than for Ar: 1.5 s at 20 K and 1 s at 60 K. It would be interesting to also consider the thermalisation of C_2^- using hydrogen as a buffer gas, particularly as it has been shown to have low reactivity with C_2^- [14]. This would also be of interest for astronomical modeling of molecular clouds or circumstellar envelopes should C_2^- ever be detected in these regions as has been suggested [49–52].

5. Conclusions

The interaction of C_2^- with the noble gases He, Ne and Ar have been calculated using *ab initio* quantum chemistry methods and

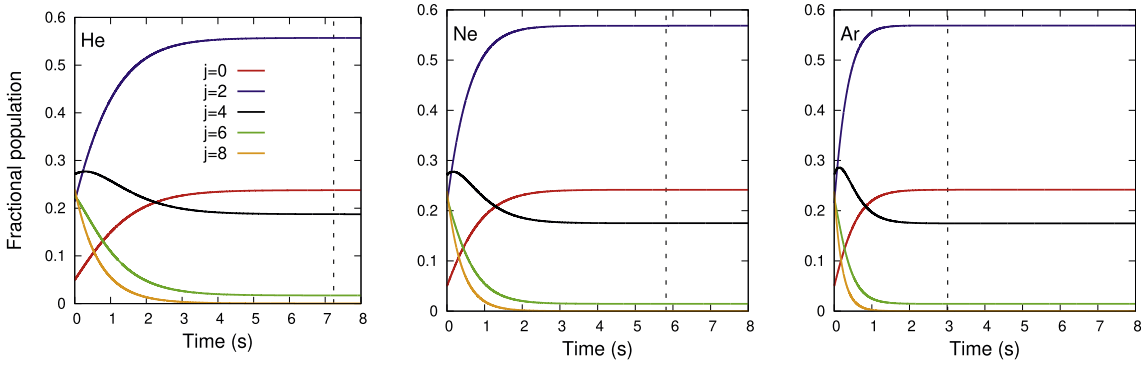

Fig. 8. Thermalisation of C_2^- rotational states during collisions with He (left panel), Ne (centre panel) and Ar (right panel) at 20 K. The colour code for the different rotational states considered in the process is reported on the left panel of the figure. Initial populations are taken from a Boltzmann distribution at 100 K. Gas pressure η chosen as 10^{10} cm^{-3}. Vertical dashed line indicates when populations reach steady state value as defined in the main text. (For interpretation of the references to colour in this figure legend, the reader is referred to the Web version of this article.)

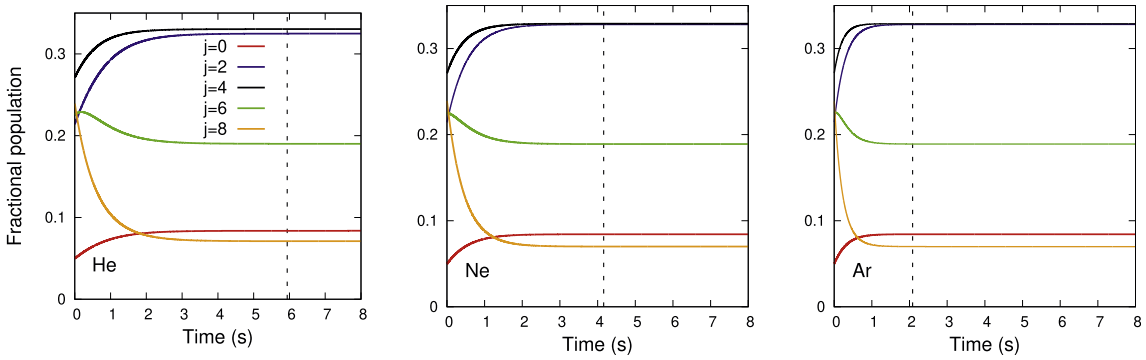

Fig. 9. Thermalisation of C_2^- rotational states during collisions with He (left panel), Ne (centre panel) and Ar (right panel) at 60 K Other parameters are the same as those of Fig. 8.

used to generate analytical potential energy surfaces. The PES have been used to carry out quantum scattering calculations to obtain rotationally inelastic scattering cross sections and corresponding rate constants. As expected, the strength of interaction of the gases with C_2^- increased in the order He < Ne < Ar due to the increasing number of electrons and polarizability of the larger atoms. The rotationally inelastic scattering cross sections increase in the same order, reflecting this stronger interaction. The rate constants broadly followed the same pattern but due to the larger mass of Ne, the rate constants for He and Ne were found here to be quite similar.

The rotational state-changing rate constants were in turn used to model the thermalisation times for C_2^- in ion traps using He, Ne or Ar as possible buffer gases. Thermalisation times were found to be quite similar for He and Ne with the latter slightly faster, while Ar was always found to be the fastest buffer gas in driving thermalisation of the rotational levels of the trapped anion.

The results presented here suggest that it is worth considering Ne and Ar as possible gases to quench the internal vibrational motion of C_2^-, a prerequisite for subsequent laser cooling experiments [25]. We have shown that for He, the vibrational quenching rate constants for $v = 2$ and $v = 1$ are very small [33] and thus cooling will be inefficient. The stronger interaction of C_2^- with Ne and Ar calculated here may also result in larger vibrational quenching cross sections and therefore allow faster cooling kinetics to the anion's $v = 0$ vibrational level.

CRediT authorship contribution statement

Barry P. Mant: Conceptualization, Investigation, Formal analysis, Writing - original draft, Software. **Franco A. Gianturco:** Conceptualization, Validation, Investigation, Writing - review & editing. **Roland Wester:** Conceptualization, Resources, Supervision, Investigation. **Lola González-Sánchez:** Methodology, Software, Investigation, Writing - review & editing. **Ersin Yurtsever:** Methodology, Investigation, Validation, Writing - review & editing, Software.

Declaration of competing interest

The authors declare that they have no known competing financial interests or personal relationships that could have appeared to influence the work reported in this paper.

Acknowledgements

F.A.G. and R.W. acknowledge the financial support from the Austrian Science Fund (FWF) (Project No. P29558−N36). L.G-S further thanks the MINECO (Spain) for the awarding of grant PGC2018-09644-B-I00.

References

[1] G. Herzberg, A. Lagerqvist, A new spectrum associated with diatomic carbon, Can. J. Phys. 46 (1968) 2363, https://doi.org/10.1139/p68-596.
[2] E.D. Milligan, M.E. Jacox, Studies of the photoproduction of the electrons in inert solid matrices. The electronic spectrum of the species C_2^-, J. Chem. Phys. 51 (1969) 1952, https://doi.org/10.1063/1.1672283.
[3] R.P. Frosch, C_2 and C_2^- spectra produced by the X irradiation of acetylene in rare-gas matrices, J. Chem. Phys. 54 (1971) 2660, https://doi.org/10.1063/1.1675229.
[4] W.C. Lineberger, T.A. Patterson, Two photon photdetachment spectroscopy: the C_2^- Σ States, Chem. Phys. Lett. 13 (1972) 40, https://doi.org/10.1016/0009-2614(72)80037-X.
[5] P.L. Jones, R.D. Mead, B.E. Kohler, S.D. Rosner, W.C. Lineberger, Photodetachment spectroscopy of C_2^- autodetaching resonances, J. Chem. Phys. 73 (1980) 4419, https://doi.org/10.1063/1.440678.
[6] S. Leutwyler, J.P. Maier, L. Misev, Lifetimes of C_2^- in rotational levels of the $B^2\Sigma_u^+$state in the gas phase, Chem. Phys. Lett. 91 (1982) 206, https://doi.org/10.1016/0009-2614(82)83642-7.
[7] R.D. Mead, U. Hefter, P.A. Schulz, W.C. Lineberger, Ultrahigh resolution spectroscopy of C_2^-: the $A^2\Pi_u$state characterized by deperturbation methods, J. Chem. Phys. 82 (1985) 1723, https://doi.org/10.1063/1.448960.
[8] B.D. Rehfuss, D.-J. Liu, B.M. Dinelli, M.-F. Jagod, W.C. Ho, M.W. Crofton, T. Oka, Infrared spectroscopy of carbo-ions, IV. The $A^2\Pi_u$–$X^2\Sigma_g^+$electronic transition of C_2^-, J. Chem. Phys. 89 (1988) 129.
[9] K.M. Ervin, W.C. Lineberger, Photoelectron spectra of C_2 and C_2H^-, J. Phys. Chem. 95 (1991) 1167, https://doi.org/10.1021/j100156a026.
[10] P. Royen, M. Zackrisson, Spin-splitting analysis of the $B^2\Sigma_u^+(v=0)$State of C_2^- using velocity modulation laster spectroscopy, J. Mol. Spectrosc. 155 (1992) 427, https://doi.org/10.1016/0022-2852(92)90534-U.
[11] H.B. Pedersen, C. Brink, A.L. H, N. Bjerre, P. Hvelplund, D. Kella, H. Shen, Experimental investigation of radiative lifetimes of vibrational levels at the electronic ground state of C_2^-, J. Chem. Phys. 464 (1998) 5849, https://doi.org/10.1063/1.477207.
[12] A.E. Bragg, R. Wester, A.V. Davis, A. Kammrath, D.M. Neumark, Excited-state detachment dynamics and rotational coherences of C_2^- via time-resolved photoelectron imaging, Chem. Phys. Lett. 376 (2003) 767, https://doi.org/10.1016/S0009-2614(03)01060-1.
[13] M. Nakajima, Observation of the $X^2\Sigma_g^+(v=4-6)$levels of C_2^-, J. Mol. Spectrosc. 331 (2017) 106, https://doi.org/10.1016/j.jms.2016.11.002.
[14] E.S. Endres, O. Lakhmanskaya, D. Hauser, S.E. Huber, T. Best, S.S. Kumar, M. Probst, R. Wester, Upper limits to the reaction rate coefficients of C_n^- and C_nH^- (n=2,4,6) with molecular hydrogen, J. Phys. Chem. 118 (2014) 6705, https://doi.org/10.1021/jp504242p.
[15] J. Barsuhn, Nonempirical calculations on the electronic spectrum of the molecular ion C_2^-, J. Phys. B Atom. Mol. Opt. Phys. 7 (1974) 155, https://doi.org/10.1088/0022-3700/7/1/025.
[16] M. Zeitz, S.D. Peyerimhoff, R.J. Buenker, A theoretical study of the bound electronic states of the C_2^- negative ion, Chem. Phys. Lett. 64 (1979) 243, https://doi.org/10.1016/0009-2614(79)80505-9.
[17] M. Dupuis, B. Liu, Theoretical study of C_2 and C_2^-, J. Chem. Phys. 73 (1980) 337, https://doi.org/10.1063/1.439879.
[18] P. Rosmus, H.-J. Werner, Multireference-CI calculations of radiative transition probabilities in C_2^-, J. Chem. Phys. 80 (1984) 5085, https://doi.org/10.1063/1.446579.
[19] J.A. Nichols, J. Simons, Theoretical study of C_2 and C_2^-:$X^1\Sigma_g^+$,$A^3\Pi_u$,$X^2\Sigma_g^+$,and $B^2\Sigma_u^+$ potentials, J. Chem. Phys. 86 (1987) 6972, https://doi.org/10.1063/1.452345.
[20] J.D. Watts, R.J. Bertlett, Coupled-cluster calculations on the C_2 molecule and

the C^{+}_2 and C^{-}_2 molecular ions, J. Chem. Phys. 96 (1992) 6073, https://doi.org/10.1063/1.4662649.
[21] T. Sedivcová, V. Spirko, Potential energy and transition dipole moment functions of C^{-}_2, Mol. Phys. 104 (2006) 1999, https://doi.org/10.1080/00268970600662689.
[22] W. Shi, C. Li, H. Meng, J. Wei, L. Deng, C. Yang, *Ab initio* study of the low-lying electronic states of the C^{-}_2 anion, Comput. Theor. Chem. 1079 (2016) 57, https://doi.org/10.1016/j.comptc.2016.01.015.
[23] M. Kas, J. Loreau, J. Liévin, N. Vaeck, Cold reactive and nonreactive collisions of Li and Rb with C^{-}_2: implications for hybrid-trap experiments, Phys. Rev. 99 (2019), 042702, https://doi.org/10.1103/PhysRevA.99.042702.
[24] S. Gulania, T.-C. Jagau, A.I. Krylov, EOM-CC guide to Fock-space travel: the C_2 edition, Farady Discuss 217 (2019) 514, https://doi.org/10.1039/c8fd00185e.
[25] P. Yzombard, M. Hamamda, S. Gerber, M. Doser, D. Comparat, Laser cooling of molecular anions, Phys. Rev. Lett. 114 (2015) 213001, https://doi.org/10.1103/PhysRevLett.114.213001.
[26] J. Fesel, S. Gerber, M. Doser, D. Comparat, Optical dipole-force cooling of anions in a penning trap, Phys. Rev. 96 (2017), https://doi.org/10.1103/PhysRevA.96.031401, 031401(R).
[27] S. Gerber, J. Fesel, M. Doser, D. Comparat, Photodetachment and Doppler laser cooling of anionic molecules, New J. Phys. 20 (2018), 023024, https://doi.org/10.1088/1367-2630/aaa951.
[28] A. Hinterberger, S. Gerber, E. Oswald, C. Zimmer, J. Fesel, M. Doser, Trapping of C^{-}_2 in a digital ion trap, J. Phys. B Atom. Mol. Opt. Phys. 52 (2019) 225003, https://doi.org/10.1088/1361-6455/ab4940.
[29] Y. Shan-Shan, Y. Xiao-Hua, L. Ben-Xi, K. Kakule, W. Sheng-Hai, G. Ying-Chun, L. Yu-Yan, C. Yang-Qin, Study of hot bands in the $B^2\Sigma^{+}_u$-$X^2\Sigma^{+}_g$ system of C^{-}_2 anion, Chin. Phys. 12 (2003) 745, https://doi.org/10.1088/1009-1963/12/7/308.
[30] M Ahmadi, et al., Observation of the 1s-2s transition in trapped antihydrogen, Nature 541 (2017) 506, https://doi.org/10.1038/nature21040.
[31] P Perez, Y Sacquin, The GBAR experiment:gravitational behaviour of antihydrogen at rest, Classical Quant. Grav. 29 (2012) 184008, https://doi.org/10.1088/0264-9381/29/18/184008.
[32] F.A. Gianturco, L. González-Sánchez, B.P. Mant, R. Wester, Modelling state-selective photodetachment in cold ion traps: rotational state ¨crowding" in small anions, J. Chem. Phys. 151 (2019) 144304, https://doi.org/10.1063/1.5123218.
[33] B. P. Mant, F. A. Gianturco, R. Wester, E. Yurtsever, L. González-Sánchez, Rovibrational Quenching of C^{-}_2 Anions in Collisions with He, Ne and Ar Atoms, In Preparation.
[34] H.-J. Werner, P.J. Knowles, G. Knizia, F.R. Manby, M. Schütz, Molpro: a general-purpose quantum chemistry program package, WIREs Comput. Mol. Sci. 2 (2012) 242–253, https://doi.org/10.1002/wcms.82.
[35] H.-J. Werner, P.J. Knowles, G. Knizia, F.R. Manby, M. Schütz, et al., Molpro, Version 2019.2, a Package of Ab Initio Programs, 2019 see, https://www.molpro.net.
[36] A.K. Wilson, T.H. van Mourik, T amd Dunning, Gaussian basis sets for use in correlated molecular calculations. vi. sextuple zeta correlation consistent basis sets for boron through neon, THEOCHEM 388 (1996) 339–349, https://doi.org/10.1016/S0166-1280(96)80048-0.
[37] D.E. Woon, T.H. Dunning Jr., Gaussian basis sets for use in correlated molecular calculations. iii. the atoms aluminum through argon, J. Chem. Phys. 98 (1993) 1358, https://doi.org/10.1063/1.464303.
[38] S.F. Boys, F. Bernardi, Calculation of small molecular interactions by differences of separate total energies - some procedures with reduced errors, Mol. Phys. 19 (1970) 553, https://doi.org/10.1080/00268977000101561.
[39] B.P. Mant, F.A. Gianturco, L. González-Sánchez, E. Yurtsever, R. Wester, Rotationally inelastic processes of C^{-}_2 ($^2\Sigma^{+}_g$) colliding with He (^{1}S) at low-temperatures: *ab Initio* interaction potential, state-changing rates and kinetic modelling, J. Phys. B Atom. Mol. Opt. Phys. 53 (2020), 025201, https://doi.org/10.1088/1361-6455/ab574f.
[40] C. Gaiser, B. Fellmuth, Polarizability of helium, neon, and argon: new perspectives for gas metrology, Phys. Rev. Lett. 120 (2018) 123203, https://doi.org/10.1103/PhysRevLett.120.123203.
[41] L. González-Sánchez, E. Yurtsever, B.P. Mant, R. Wester, F.A. Gianturco, Collision-driven state-changing efficiency of different buffer gases in cold traps: He(^{1}S) Ar (^{1}S) and p-H2($^1\Sigma$) on trapped CN^{-}($^1\Sigma$), Phys. Chem. Chem. Phys. Advance Article (2020), https://doi.org/10.1039/d0cp03440a.
[42] D. López-Duránn, E. Bodo, F.A. Gianturco, ASPIN: an all spin scattering code for atom-molecule rovibrationally inelastic cross sections, Comput. Phys. Commun. 179 (2008) 821, https://doi.org/10.1016/j.cpc.2008.07.017.
[43] M.H. Alexander, Rotationally inelastic collisions between a diatomic molecule in a $^2\Sigma^{+}$electronic state and a structureless target, J. Chem. Phys. 76 (1982) 3637.
[44] A.M. Arthurs, A. Dalgarno, The theory of scattering by a rigid rotator, Proc. R. Soc. A 256 (1960) 540, https://doi.org/10.1098/rspa.1960.0125.
[45] D.E. Manolopoulos, An improved log derivative method for inelastic scattering, J. Chem. Phys. 85 (1986) 6425, https://doi.org/10.1063/1.451472.
[46] R. Martinazzo, E. Bodo, F.A. Gianturco, A modified variable-phase algorithm for multichannel scattering with long-range potentials, Comput. Phys. Commun. 151 (2003) 187, https://doi.org/10.1016/S0010-4655(02)00737-3.
[47] O.Y. Lakhmanskaya, T. Best, S.S. Kumar, E.S. Endres, D. Hauser, R. Otto, S. Eisenbach, A. von Zastrow, R. Wester, Properties of a multipole ion trap studied by evaporative ion losses, Int. J. Mass Spectrom. 365–366 (2014) 281–286, https://doi.org/10.1016/j.ijms.2014.03.001.
[48] J. Mikosch, H. Kreckel, R. Wester, R. Plašil, J. Glosik, D. Gerlich, D. Schwalm, A. Wolf, Action spectroscopy and temperature diagnostics of H^{+}_3 by chemical probing, J. Chem. Phys. 121 (2004) 11030, https://doi.org/10.1063/1.1810512.
[49] M.S. Vardya, K.S. Krishna Swamy, Can lines of C^{-}_2 be observed in carbon stars? Chem. Phys. Lett. 73 (1980) 616, https://doi.org/10.1016/0009-2614(80)80730-5.
[50] T. Faÿ, H.R. Johnson, A search for C^{-}_2 in spectra of HD201626 and the sun, PASP 84 (1972) 284, https://doi.org/10.1086/129284.
[51] G. Wallerstein, A search for C^{-}_2 in the hydrogen-poor carbon star HD 182040, Astron. Astrophys. 105 (1982) 219.
[52] S. Civis, Y. Hosaki, E. Kagi, H. Izumiura, K. Yanagisawa, T. Sedivcová, K. Kawaguchi, Search for C^{-}_2 in diffuse clouds, Publ. Astron. Soc. Jpn. 57 (2005) 605, https://doi.org/10.1093/pasj/57.4.605.